



Shore Protection Using Special Perforated Breakwater with Generating Renewable Energy

Yasser El Saie*

Department of Civil Engineering, Higher Institute of Engineering, Cairo, Egypt

ABSTRACT

This paper presents an innovative vertical perforated breakwater for protecting the shoreline from sea water wave energy and converting the transmitted water wave energy to renewable energy through vents inside the body. This structure is composed of a vertically faced rectangular shape with a number of vents that differ from some ratios of porosities tested first as a wave energy dissipater by warning the wave height sensors before and after the seawall and analyzing the total energy transmitted to push it to an innovative system producing renewable electric energy by adapting the location of these vents and changing the dimensions of these holes in three models with dimensions (8 × 4, 4 × 4, and 7 × 6, respectively, dimensions in cms). By choosing five heights of water depths (15, 19, 23, 27 and 31 cms) and four eccentricities of the wave maker, we also recorded the volt and ampere and finally the total percentage of wave energy that could be converted. These experiments were carried out in a recirculating open channel flume located at the Hydraulics Engineering Laboratory at the Higher Institute of Engineering in El Shorouk City.

Key Words: Special perforated breakwater; Transmitted water wave energy; Shore protection; Water wave energy converter and renewable energy

INTRODUCTION

Important ports with many economic activities are located along the sea coasts; therefore, breakwaters are usually built to protect the beaches against waves and floods, especially if these coastal areas have a high population density. In this paper, three models of coastal structures will be tested. A new concept for wave dissipation and conversion energy is examined to prove the concept for generating electricity using three different physical models. Vertical Seawall with different porosities to analyze the preliminary efficiency of these devices.

Economic expansion continuously requires additional construction Seawalls to protect the shoreline, and it could be possible to include some changes inside the body of the wall to generate energy. Concrete blocks are usually used in breakwaters, which are placed in front of the vertical breakwater and dissipate part of the energy of the incoming wave. The energy dissipation efficiency of the perforated structure can be direct-

ly evaluated by reflecting and absorbing the wave from the breakwater. Due to the complex properties that depend on the interaction between the waves and the porous medium of the breakwater body, three laboratory models were used to verify the reflection, absorption and crash of the wave on the tested breakwater body. To explore the characteristics of wave interactions with porous structures, many numerical models based on the Navier-Stokes equations were presented by using numerical techniques, such as Dalrymple et al.(1991) [1]. For the interaction between the permeable structure and water waves, which is able to consider wave breaking in a three dimensional wave field, [2]? The field of flow caused by the movement of the waves and the movement of water molecules in and around the vertical permeable structure, which is affected by the interaction between the waves and the porous medium of the barrier body, was investigated. Therefore, a fully nonlinear three dimensional numerical model has been developed to study these interactions between waves and wave barriers

Received:	01-August-2022	Manuscript No:	lpbjr-22-14057
Editor assigned:	03-August-2022	PreQC No:	lpbjr-22-14057 (PQ)
Reviewed:	17-August-2022	QC No:	lpbjr-22-14057
Revised:	22-August-2022	Manuscript No:	lpbjr-22-14057(R)
Published:	29-August-2022	DOI:	10.21767/2394-3718-9.8.100

Corresponding author Yasser El Saie, Department of Civil Engineering, Higher Institute of Engineering, Cairo, Egypt, E-mail: yasser_elsaie@yahoo.com

Citation Saie EY (2022) Shore Protection Using Special Perforated Breakwater with Generating Renewable Energy. Br J Res Vol.9:100

Copyright © Saie EY. This is an open-access article distributed under the terms of the Creative Commons Attribution License, which permits unrestricted use, distribution, and reproduction in any medium, provided the original author and source are credited.

that have a percentage of permeability [3]. Describing how to apply a numerical model to a partially perforated vertical wall caisson and irregular waves. By testing the performance of this model, existing experimental data are used for regular waves, while a laboratory experiment is conducted in this study for irregular waves [4]. The numerical results are validated with the experimental data of surface elevations and wave pressures acting on the caisson breakwater [5]. Proposes a new concept for a system of wave energy conversion. The objective of this research was to create and test a new system for wave energy converters that can be integrated within a breakwater. In this new concept, the primary function of this device will remain the protection of the harbor [6]. The hydrodynamic efficiency of the seawall is presented as a function of the wave run up, reflection, and energy dissipation coefficients. Different wave and structural parameters affecting the seawall efficiency are investigated by El-Sadek M. Heikal, et al. (2012) [7].

Qualitative progress is introduced with three dimensional models, which are not so limited because they reproduce full 3D wave transformation processes, such as diffraction, which typically occur on breakwater heads [8]. Four different simple, single porous vertical blocks were tested using regular waves. These additional tests represent slightly more complex configurations, including double blocks, reflective boundaries, irregular waves and sloping structures [9]. The interaction between the wave and the partial perforated caisson in a 2D numerical wave flume is investigated by means of the renewed SPH algorithm, and the mathematical equations are reform of SPH numerical approximation based on Navier-Stokes equations [10]. A review and validation of control strategies for massive wave energy conversion systems, briefly outlines the characteristics of ocean wave energy, and summarizes the principles of ocean and sea energy aggregation by studying the specific wave energy transformers and commercial devices deployed in the real sea between 2005 and 2016, Liguó et al. (2017) [11]. Wave energy enhancement for nearshore electricity generation [12]. For examiner of the process of advanced ocean environment replication starting from the sea and ending to the tank, and rather than an exhaustive overview of all approaches, it follows the rationale behind projects led [13]. The generation of renewable energy in transition is energy and economic cost. Southeast Asia therefore has several enormous potentials for its sustainable energy sources. However, to date, they have not yet performed globally ahead in renewable energy deployment due to various challenges [14]. An innovative vertical breakwater cross-section integrating an overtopping wave energy converter, named OBREC-V, and the analysis of its hydraulic performance and stability response to hydraulic loading. The structure consists of a vertically faced caisson with a sloping ramp on the top, a reservoir and a set-back crown-wall, Enrico Di Lauro, et al. (2020) [15].

MATERIALS AND METHODS

Experimental Wave Flume

Experiments were performed in a steel and glass wave flume 12.0 m long, 50 cm wide and 60 cm deep. The sidewalls are 12.00 glass panels, each of which is one meter in a Skelton steel frame, with a wave maker used is fly wheel type connected by

steel rod to paddle located at the beginning of the flume to generate waves with variable heights and lengths as shown in **Figure 1**. The wave period, length and height are measured by a Sonic Wave Sensor XB. When mounting the Sonic Wave Sensor XB, a level should be used to assure that it is vertical. The basic operating principle is to measure the ultra sound travel time. The result is then scaled with a Micro Processor in the unit, and then it is transmitted over the Xbee wireless network to an Xbee USB adapter. A Windows USB to Serial Converter connects the USB Adapter port to the User Interface Software (GUI).



Figure 1: Shape of the experimental wave flume

The wave staff XB was installed in three positions to indicate incident, reflection, and transmission wave heights. The instrument was mounted on a small steel frame moves on the sides of the flume. The spacing between wave gauges applied was based on Mansard and Funke (1980) [16]. suggestions to calculate the relative distances between wave gauges. $X_{12}=L/10$, $L/6 \leq X_{13} \leq L/3$, Where L is the wavelength, X_{12} is the distance between the first two gauges positions and X_{13} is the distance between the first and third wave gauges in the line of wave propagation as shown in **Figures 2 and 3**.



Figure 2: Elevation and plan of the experimental wave flume

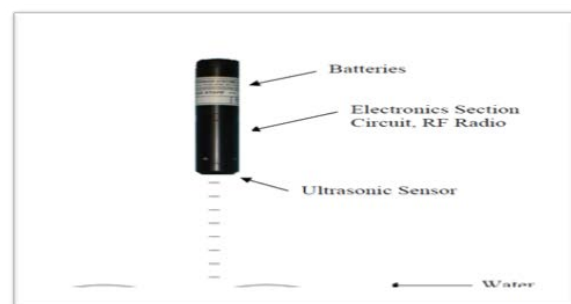


Figure 3: Shape of sonic wave sensor XB

Design of the Three Special Physical Breakwater Models

The physical models consist of three models of a constant height 50 cm, constant depth 20 cm and 49 cm width. The first model has five vents each (8.0×4.0 cms), the second model has five vents each (4.0×4.0 cms) and the third model has four vents each (7.0×6.0 cms). All of these vents have spacing 5.0

cm from each other and start 15 cm from bed level, as shown in the upstream sides of the three models (Figures 4-6). These vents take an inclined shape in the body of the models such as sloped tunnels (36° with horizontal) downwards to reduce the transmitted energy downstream of these models, as shown in Figures 7-9.



Figure 4: Model 1



Figure 5: Model 2



Figure 6: Model 3

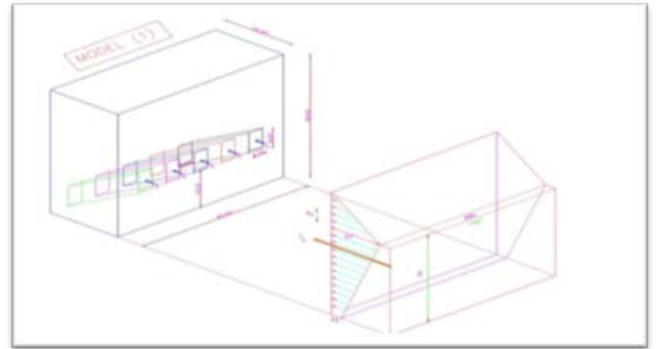


Figure 7: Model (1) with five tunnels and impact pressure distribution

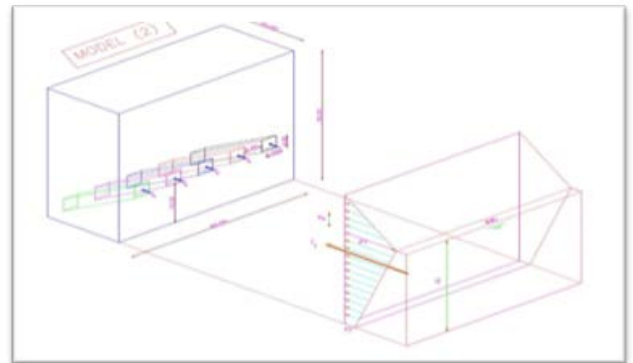


Figure 8: Model (2) with five tunnels and impact pressure distribution

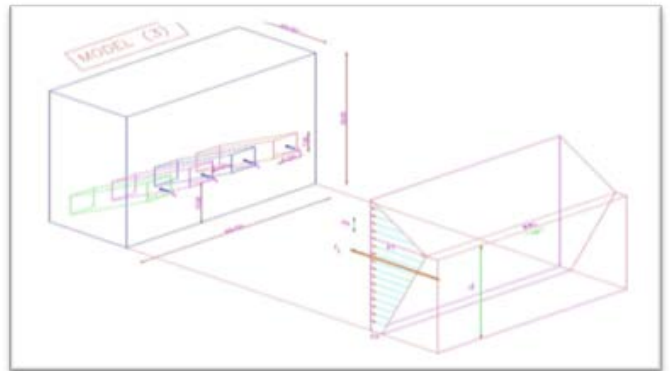


Figure 9: Model (3) with five tunnels and impact pressure distribution

Measuring and Calculating Data

The measurements were tabulated. The incident and reflected waves were calculated from the Sonic Wave Sensor XB for the three tested models as follows:

$$H_i = (H_{max} + H_{min}) / 2 \tag{1}$$

$$H_r = (H_{max} - H_{min}) / 2 \tag{2}$$

Where:

Hi: Incident wave height.

Hr: Reflected wave height.

The dissipated wave energy was calculated for every tested case based on the following relation:

$$E_i = E_r + E_t + E_d = (1/8 \times \rho \times g \times H^2) \tag{3}$$

Where

E_i=Incident energy
 E_r=Reflected energy
 E_t=Transmitted energy
 E_d=Dissipated energy

Additionally, the coefficients of transmission, reflected and dissipation were calculated (C_t, C_r and C_d), wave length and the percentage of energy transmitted, as shown for model one, as an example in **Table 1**.

Table 1: Measuring and calculating terms & % of energy transmitted

Ecc. of Wave maker	Water depth (cm)	Hins. (cm)	Htrans. (cm)	Href. (cm)	L (cm)	Ct	Cr	Cd	% Energy transmitted
Case1	31	8.54	1.77	0.93	156.341	0.207	0.109	0.972	4.296
	27	6.785	1.52	0.599	146.452	0.224	0.088	0.971	5.018
	23	6.195	1.43	0.511	141.365	0.231	0.083	0.969	5.328
	19	5.11	1.31	0.43	128.365	0.256	0.084	0.963	6.572
	15	2.455	0.38	0.275	118.254	0.155	0.112	0.982	2.396
Case2	31	8.155	1.32	0.425	141.258	0.162	0.067	0.985	2.62
	27	6.575	1.19	0.425	130.584	0.181	0.065	0.983	3.276
	23	5.888	1.03	0.313	128.369	0.175	0.053	0.978	3.061
	19	4.705	0.95	0.465	110.258	0.202	0.099	0.974	4.077
	15	3.86	0.23	0.18	98.254	0.072	0.047	0.997	0.355
Case3	31	7.745	1.02	0.375	127.325	0.098	0.048	0.993	2.335
	27	7.133	0.86	0.325	117.256	0.093	0.325	0.993	1.66
	23	5.485	0.71	0.435	102.145	0.087	0.435	0.992	1.676
	19	4.43	0.63	0.23	90.247	0.087	0.23	0.995	2.022
	15	3.35	0.19	0.15	78.569	0.043	0.15	0.998	0.322
Case4	31	5.19	0.51	0.5	115.365	0.098	0.096	0.993	0.966
	27	4.51	0.42	0.33	103.147	0.093	0.073	0.993	0.867
	23	3.565	0.31	0.325	88.781	0.087	0.091	0.992	0.756
	19	2.975	0.26	0.125	79.256	0.087	0.042	0.995	0.764
		2.55	0.11	0.1	76.254	0.043	0.039	0.998	0.186

Additionally, the total impact force exerted in the vertical breakwater and its location from the bed level of the experimental flume is determined from the Sainflou method as follows (**Figure 10**):

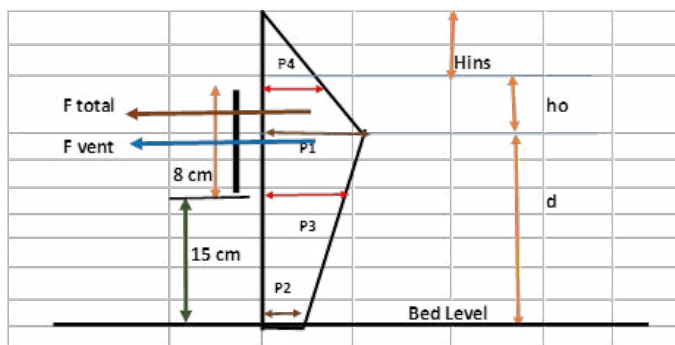


Figure 10: Pressure distribution acting on the special vertical seawall (Sainflou)

$$h_o = \frac{\delta H^2}{L} \coth\left(\frac{2\delta d}{L}\right)$$

$$h_o = \frac{\delta H^2}{L} \coth\left(\frac{2\delta d}{L}\right)$$

$$P_2 = \frac{\tilde{a}_{s,w} \times H}{\cosh\left(\frac{\delta d}{L}\right)}$$

Where

h_o=Height of average wave period over mean water level (cm).

H=Incident wave height (cm).

L=Wave length (cm).

d=Water depth (cm).

P₁=Pressure of the impact wave at the mean water level (gm/cm²).

P₂=Pressure of the impact wave at the bed flume level (gm/cm²).

γ_{sw}=Specific weight of salt water (gm/cm³).

P₃=Pressure of the impact wave at the lower end of the vent (gm/cm²).

P₄=Pressure of the impact wave at the higher end of the vent (gm/cm²).

F_{total}=The resultant force/m acting on the vertical breakwater (gm).

F_{vent}=The resultant force acting on one vent in the vertical breakwater (gm).

So, for example model one we can calculate the total force that was acting on the breakwater and the location from the bed level, also the force acting on one vent and the percentage of force acting for one vent to the total force acting on the vertical breakwater as shown in **Tables 2 and 3** for model one with

different eccentricities of the wave maker (4 cases) and we can neglect the records at depth 15.00 cm because these records seems negligible compared with the others, as the water level be the same level of the lower end of the vent.

Likewise, for model two five vents each (4.0 × 4.0) cms with spacing 5.0 cm and model three four vents each (7.0 × 6.0) cms with spacing 5.0 cm the same tables done in the lab.

Table 2: For model (1) case (1 and 2)

Item	Case (1) Wave maker ecc. 1				Case (2) Wave maker ecc. 2			
	31	27	23	19	31	27	23	19
d (cm)	31	27	23	19	31	27	23	19
ho (cm)	1.73	1.2	1.11	0.87	1.68	1.21	1.05	0.79
Hins (cm)	8.54	6.79	6.2	5.11	8.16	6.58	5.89	4.71
d (cm)	31	27	23	19	31	27	23	19
P1 (gm/cm2)	8.84	7.05	6.49	5.39	8.4	6.79	6.13	4.91
P2 (gm/cm2)	4.54	3.88	3.95	3.49	3.87	3.34	3.46	2.86
P3 (gm/cm2)	6.62	5.41	5.59	4.98	6.53	5.25	5.19	4.22
P4 (gm/cm2)	7.73	6.3	6.21	5.31	7.96	6.37	6.13	5.07
Fvent (gm)	57.4	49.65	47.2	41.16	57.96	46.48	45.28	37.16
Ftotal on wall (gm)	252.87	175.74	143.78	100.46	231.34	163.15	131.51	87.28
Position from bed (cm)	20.26	17.19	14.58	11.91	20.42	17.39	14.63	11.96
% Fv/Ft	22.7	28.25	32.83	40.97	25.05	28.49	34.43	42.58

Table 3: For model (1) case (3 and 4)

Item	Case (3) Wave maker ecc. 3				Case (4) Wave maker ecc. 4			
	31	27	23	19	31	27	23	19
d (cm)	31	27	23	19	31	27	23	19
ho (cm)	1.63	1.33	1.04	0.79	0.79	0.67	0.47	0.4
Hins (cm)	7.75	6.68	5.49	4.43	5.19	4.51	3.57	2.98
d (cm)	31	27	23	19	31	27	23	19
P1 (gm/cm2)	7.94	6.86	5.64	4.57	5.31	4.61	3.59	3.1
P2 (gm/cm2)	3.21	2.98	2.52	2.21	1.86	1.68	1.33	1.28
P3 (gm/cm2)	5.48	5.14	4.55	4.06	3.53	3.36	2.81	1.43
P4 (gm/cm2)	6.71	6.29	5.64	4.56	4.41	4.08	3.59	2.34
Fvent (gm)	48.76	45.72	40.76	34.48	31.76	29.76	25.6	20.57
Ftotal on wall (gm)	209.97	160.25	112.23	76.26	126.94	96.92	63.8	46.89
Position from bed (cm)	20.6	17.74	14.97	12.19	19.86	17.22	14.51	11.87
% Fv/Ft	23.22	28.53	36.32	45.21	25.02	30.7	40.12	43.87

RESULTS AND DISCUSSION

After studying the results of the experiments for the different three models, we can analyze these results in some curves and column charts as follows beginning with model one:

Figures 11 and 12 show that the wave steepness (H_i/L) is inversely proportional to C_t for different eccentricities and different depths of water and show why we can neglect records for a depth of 15.00 cm because the transmitted energy is very low for different H_i/L values compared to the other depths.

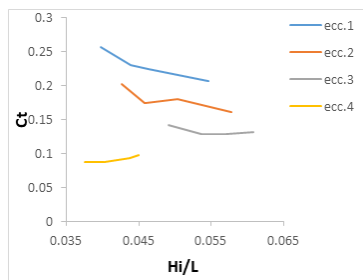


Figure 11: Relationship between C_t & H_i/L

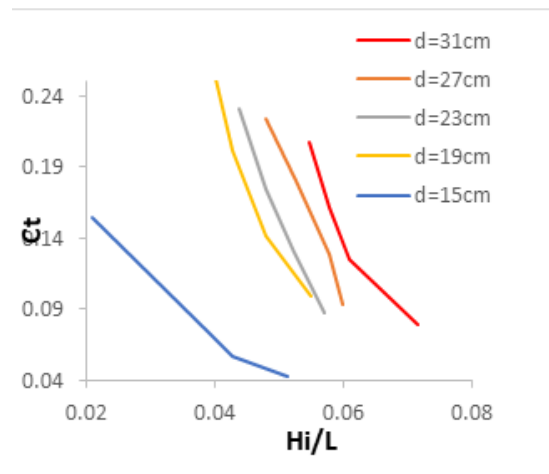


Figure 12: Relationship between C_t & H_i/L

Figure 13 shows the direct proportion between H_i/L and C_d for different depths, and Figure 14 shows the inverse proportion between H_i/L and % of energy transmitted.

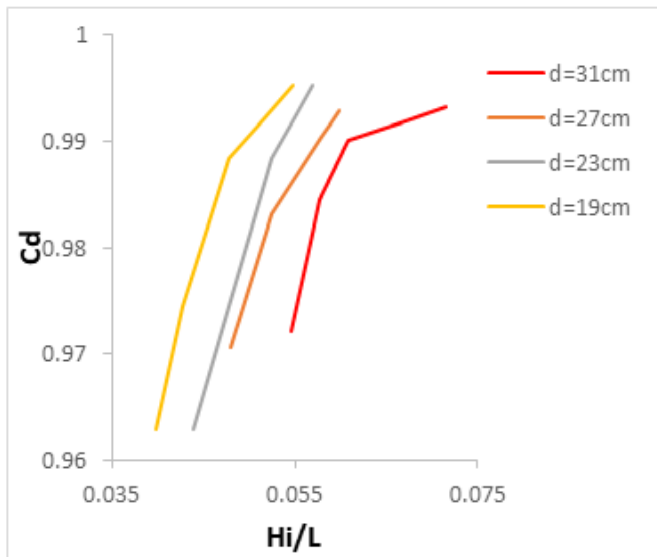


Figure 13: Relationship between Cd and Hi/L

proportion, but in Figure 17 the relation is directly proportion between Hi/L and Cd.

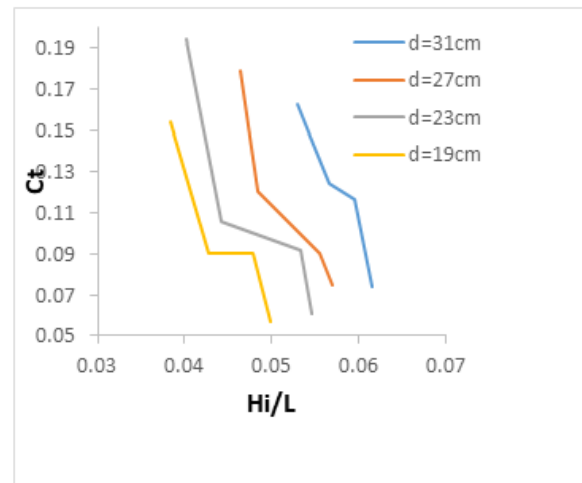


Figure 16: Relationship between Ct & Hi/L

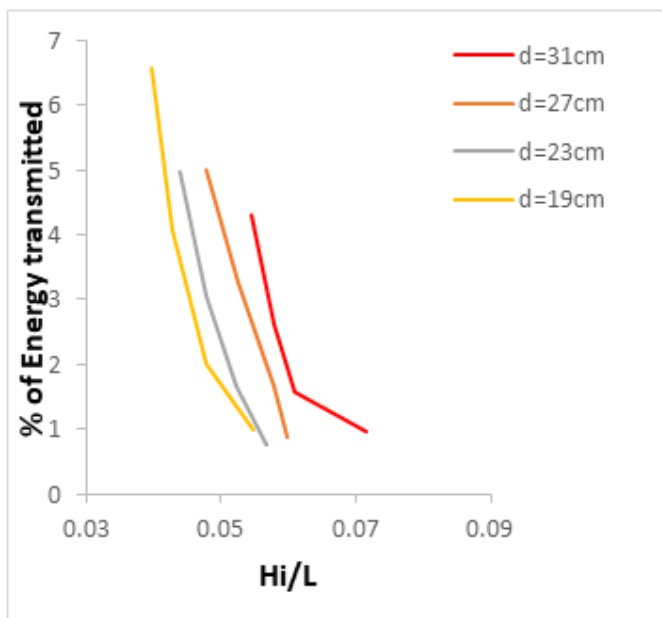


Figure 14: Relationship between % Ener. Trans. & Hi/L

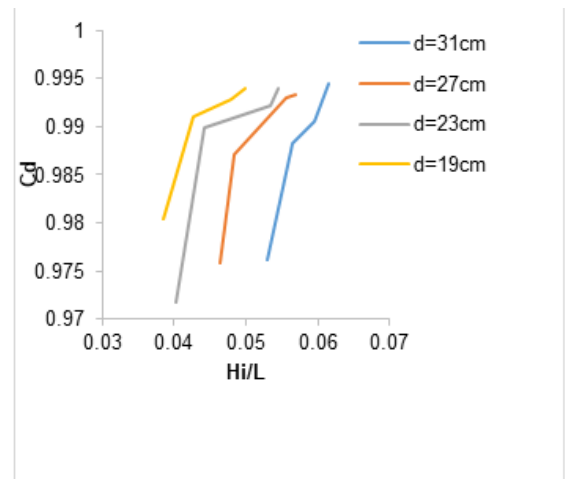


Figure 17: Relationship between Cd & Hi/L

For Figure 15, the relation between Hi/L and the percentage of force on the vent to the total force on the breakwater (Fv/Ft) is inversely proportional for different depths and eccentricities.

For Figure 18, the relation between Hi/L and % of energy transmitted is inversely proportional, and Figure 19 shows that the percentage of force on the vent to the total force on the vertical wall (Fv/Ft) is inversely proportional to the wave steepness (Hi/L) for different depths and eccentricities.

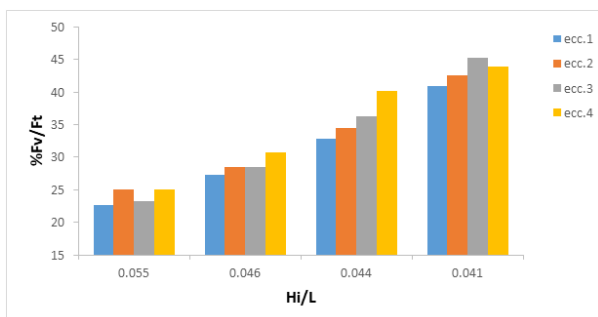


Figure 15: Relation between % of Fv/Ft & Hi/L

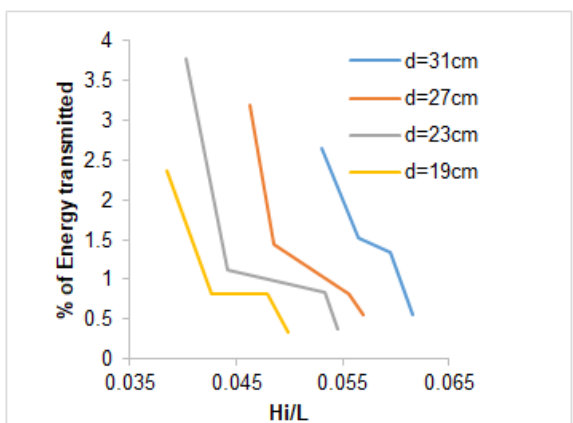


Figure 18: Relation between % Ener. Trans. & Hi/L

Additionally, for model two, the curves and column charts can be shown as follows:

Finally, for the third model, the curves and charts are shown as follows:

For Figure 16, the relation between Hi/L and Ct is inversely

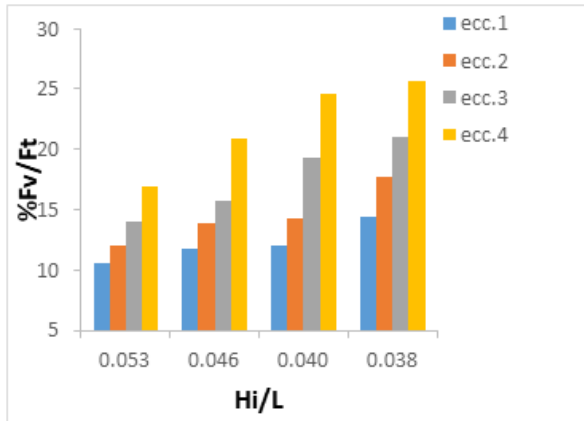


Figure 19: Relation between % Fv/Ft & Hi/L

For Figure 20, the relation between Hi/L and Ct is inversely proportion, but in Figure 21 the relation is directly proportion between Hi/L and Cd.

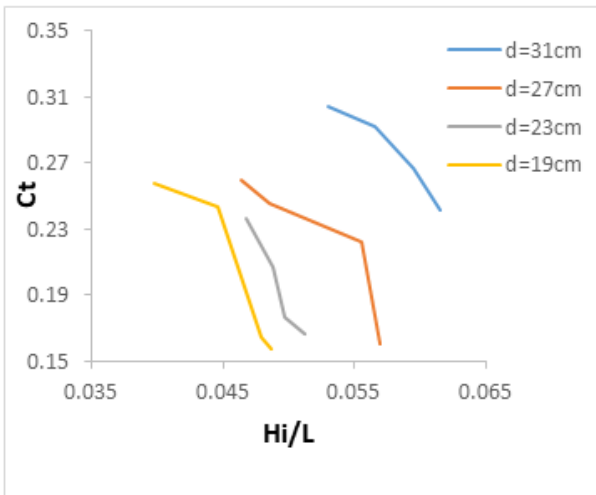


Figure 20: Relationship between Ct & Hi/L

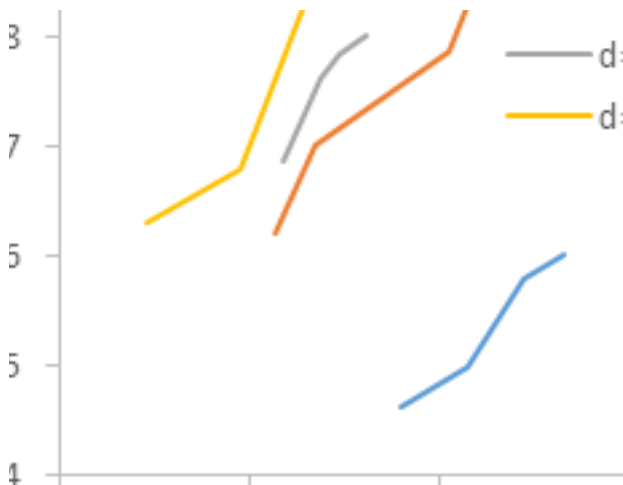


Figure 21: Relationship between Cd & Hi/L

For Figure 22, the relation between Hi/L and % of energy transmitted is inversely proportional, and Figure 23 shows that the percentage of force on the vent to the total force on the vertical wall (Fv/Ft) is inversely proportional to the wave steepness (Hi/L) for different depths and eccentricities.

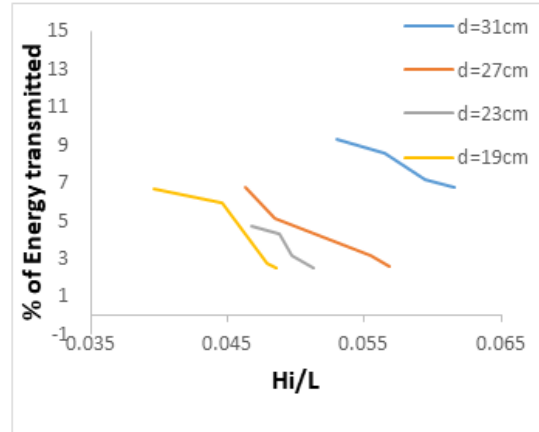


Figure 22: Relation between % Ener. Trans. & Hi/L

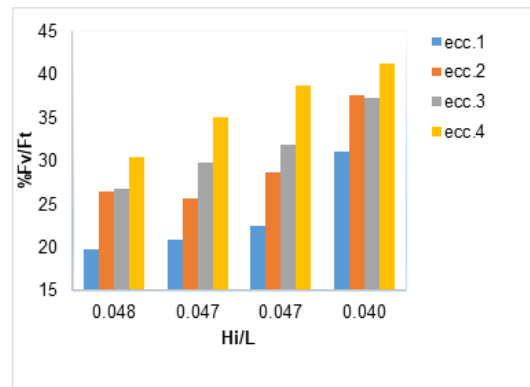


Figure 23: Relation between %Fv/Ft & Hi/L

Using the Three Models as an Electrical Energy Generator

To benefit from the percentage of energy transmitted downstream in the models, we put a small generator at the lower end of the vent to produce renewable electric energy from this transmitted water wave energy and connect these generators by an avometer to measure the voltage and the ampere that can be produced from the transmitted wave energy.

Figures 24 show the generators at the end of the tunnel in the body of the models by measuring either of the transmitted wave downstream models after generating electricity, the total power in every case is calculated and compared with the real power, as shown in Table 4, as shown below.

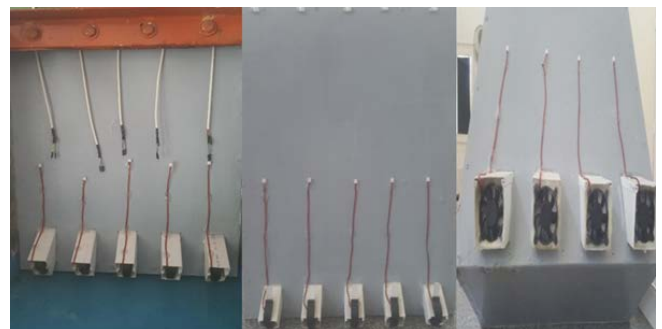


Figure 24: Generators

For models one and two, the flow of water is parallel to the fan in the small generator, but in model three, the flow of the

water is perpendicular to the fan in the generator to compare any of them are more effective in generating renewable electrical power.

Therefore, these column charts can easily discuss the compar-

Table 4: Measured and calculated terms for generating electrical power in model one

Hi/L	d (cm)	Htrans (cm)	Volt *10 ⁻³	*10 ⁻⁶	Power *10 ⁻⁹ Watt	No. of vents	Total volt *10 ⁻³	Total Amperre *10 ⁻⁶	Generat-ed Power *10 ⁻⁶ Watt	Real Generated Power Watt
0.055	31	0.68	150	3.5	525	5	750	17.5	13.125	5.127
0.058		0.53	101	2.35	237		505	11.75	5.934	2.318
0.061		0.41	78	1.62	126		390	8.1	3.159	1.234
0.072		0.33	65	1.28	83		325	6.4	2.08	0.813
0.048	27	0.57	210	4.2	882		1050	21	22.05	8.613
0.053		0.5	138	2.87	396		690	14.35	9.902	3.868
0.058		0.35	115	2.15	247		575	10.75	6.181	2.415
0.06	23	0.21	98	1.51	148		490	7.55	3.7	1.445
0.044		0.47	314	4.8	1507		1570	24	37.68	14.719
0.048		0.39	298	3.14	936		1490	15.7	23.393	9.138
0.052		0.31	179	2.68	480		895	13.4	11.993	4.685
0.057	19	0.15	121	1.89	229		605	9.45	5.717	2.233
0.04		0.41	418	5.23	2186		2090	26.15	54.654	21.349
0.043		0.36	312	3.97	1239		1560	19.85	30.966	12.096
0.048	19	0.27	236	3.14	741		1180	15.7	18.526	7.237
0.055		0.09	189	2.25	425	945	11.25	10.631	4.153	

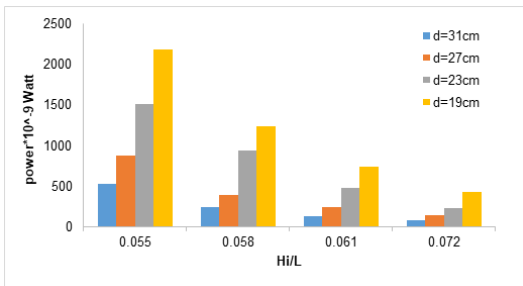


Figure 25: Relation between generating power & Hi/L in model one

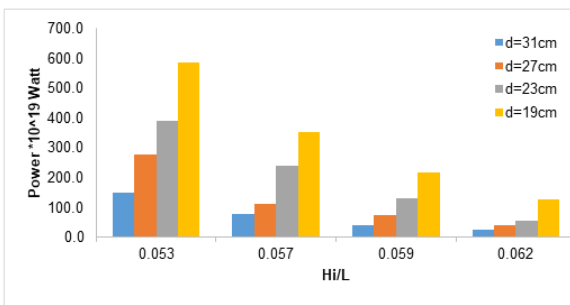


Figure 26: Relation between generating power & Hi/L in model two

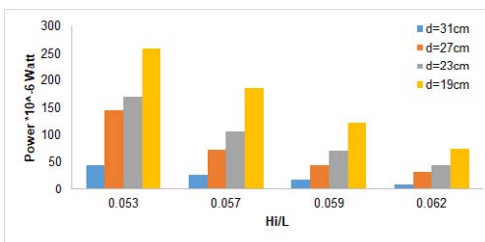


Figure 27: Relation between generating power & Hi/L in model three

ison between the three models in generating electrical power, as shown in **Figures 25-27**.

From **Figures 25-27**, the relation between Hi/L and the percentage of the generated power is inversely proportional, and the maximum generated power is located in model one, where the flow is parallel to the van that is located inside the generator, and the minimum generated electric power when the flow of water is perpendicular to the van inside the generator. Additionally, the area of the vent is directly proportional to the electrical power generated through all three models.

CONCLUSIONS AND RECOMMENDATIONS

Part 1

To evaluate the performance of using this Vertical Perforated breakwater for Protecting Shoreline for the three tested models, the conclusions of these experiments are as follows:

1) For the three models, the relation between wave steepness (Hi/L) and coefficient of transmission (Ct) are inversely proportional for different depths and eccentricities, so the ratios are as follows:

For model one, Hi/L ranged between 0.04 and 0.078, the corresponding Ct ranged between 0.24 and 0.09; for model two, Hi/L ranged between 0.04 and 0.06, the corresponding Ct ranged between 0.19 and 0.06; and for model three, Hi/L ranged between 0.04 and 0.063, the corresponding Ct ranged between 0.3 and 0.15.

2) For the three models, the relation between wave steepness (Hi/L) and the coefficient of dispersion (Cd) are directly proportional for different depths and eccentricities, so the ratios are as follows:

For model one, H_i/L ranged between 0.04 and 0.078, the corresponding C_d ranged between 0.96 and 0.994; for model two, H_i/L ranged between 0.04 and 0.06, the corresponding C_d ranged between 0.97 and 0.995; and for model three, H_i/L ranged between 0.04 and 0.063, the corresponding C_d ranged between 0.963 and 0.987.

3) For the three models, the relation between wave steepness (H_i/L) and % of energy transmitted are inversely proportional for different depths and eccentricities, so the ratios are as follows:

For model one, H_i/L ranged between 0.04 and 0.078, the corresponding % of energy transmitted ranged between 1.0 and 7.0%; for model two, H_i/L ranged between 0.04 and 0.06, the corresponding % of energy transmitted ranged between 0.5 and 3.5%; and for model three, H_i/L ranged between 0.04 and 0.063, the corresponding % of energy transmitted ranged between 2.5 and 9.0%.

4) For the three models, the relation between wave steepness (H_i/L) and the ratio force on the vent to the total force on the vertical wall (F_v/F_t) are inversely proportional for different depths and eccentricities, so the ratios are as follows:

For model (1), H_i/L ranged between 0.04 and 0.078, the corresponding (F_v/F_t) % ranged between 22.0 and 45.0%; for model two, H_i/L ranged between 0.04 and 0.06, the corresponding (F_v/F_t) % ranged between 10.0 and 26.0%; and for model three, H_i/L ranged between 0.04 and 0.063, the corresponding (F_v/F_t) % ranged between 19.0 and 43.0%.

Therefore, model (2) has the minimum energy transmitted, which means that the area of the vent is directly proportional to the % of energy transmitted, and model two has the maximum energy transmitted.

Part 2

Generating renewable electric power through vents from the transmitted water wave energy:

1) Model (1) can produce maximum electric power from one equal vent (2090×10^{-9} watts) at minimum wave steepness (H_i/L)=0.055; model (2) can produce maximum electric power from one vent (585×10^{-9} watts) at minimum wave steepness (H_i/L)=0.053; and model (3) can produce maximum electric power from one vent (259×10^{-9} watts) at minimum wave steepness (H_i/L)=0.053.

This means that the maximum area of the vent leads to maximum generated electric energy and is located nearly when the mean water level is at the center of the vent. Therefore, the direction of the flow parallel to the generating vane is more effective than that located perpendicular to the direction of the flow.

For further recommendations studying the change of the slope inside the tunnel in the vertical wall to be horizontal at the finishing trials, change the cross section of the vent to be circular section and finally increase the rows of vents above mean water level for more generating electric power.

REFERENCES

- Dalrymple RA, Martin PA (1991) Reflection and transmission from porous structures under oblique wave attack. *J Fluid Mech* 224(3):625–644.
- Mizutani N, Mostafa AM (2000) Wave-induced flow in a porous vertical breakwater. *ISOPE* (3):625-632.
- Aliasghar G, Norimi M, Dong SH (2003) Three-dimensional analysis of nonlinear interaction between water waves and vertical permeable breakwater. *J Coast Eng* 45(1):1-28.
- Kyung DS, Jae KP, Woo SP (2004) Wave reflection from partially perforated-wall caisson breakwater. *Ocean Eng* 33(2):264–280.
- Chiu, Lee JY, Chang SC, Lin YJ, Chen CH, et al. (2007) An experiment study of wave forces on vertical breakwater. *J Mar Sci Tech* 15(3):158–170.
- Joris S, Bas R, Han V, Wilfred M, Erik TO, et al. (2010) Generating electricity at a breakwater in a moderate wave climate. *Coast Eng.* 1(32)
- Sadek M, Heikal , Ayman S, Koraim, Ahmed A, et al.(2012) Protecting coasts against probable sea level rise using vertical porous sea wall. *J Eng Sci Technol* 15(3): 223-233.
- Del J, Lara M, Losada JL, (2012) Three-dimensional interaction of waves and porous coastal structures. part i: Numerical model formulation. *Coast Eng* 64(5): 57–72.
- Jeroen VDB, Gerben JV, Henk JV, Coen K (2014) Reflection and transmission through a vertical, permeable breakwater. *Commun Hydraulic Geotech Eng*
- Jiang F, Tang XC, JIN Z, ZHANG L, Chen Hz, (2015) Numerical method for wave forces acting on partially perforated caisson. *China Ocean Eng* 29(2):197-208.
- Liguo W, Jan I, Elisabetta T (2017) Review of control strategies for wave energy conversion systems and their validation. *Renew Sustain Energy Re* 81(1):366-379.
- Jagath KDR, Dias DD, Nawagamuwa RL, Weerasinghe WMAR (2018) Wave energy enhancement for nearshore electricity generation. *J Inst Eng I.I* (02):43-52.
- Draycott S, Sellar B , Davey T, Noble DR, Venugopal V, et al.(2019) Capture and simulation of the ocean environment for offshore renewable energy. *Renew Sustain Energy Rev* 104(1):15–29.
- Erdiwansyah, Mamat R, Sani MSM, Sudhakar K (2019) Renewable energy in southeast asia: Policies and recommendations. *Sci Total Environ* 20 (670):1095–1102.[PubMed]
- Enrico DL, Maria M, Javier LL, Inigo J, Losada, et al. (2020) Advantages of an innovative vertical breakwater with an overtopping wave energy converter. *Coast Eng* 159(1): 103-713.
- Mansard EPD, Funke ER (1980) The measurement of incident and reflected spectra using a least squares method. *Coast Eng* 17(1):54-172.